Effects of grown-in defects on interdiffusion dynamics in InAs/InP(001) quantum dots subjected to rapid thermal annealing

C. Dion,[1,a)] P. Desjardins,[1] N. Shtinkov,[2] F. Schiettekatte,[3] P. J. Poole,[4] and S. Raymond[4]
[1]*Regroupement Québécois sur les Matériaux de Pointe (RQMP), Département de Physique, Université de Montréal, Montréal, Québec H3C 3J7, Canada*
[2]*Physics Department, University of Ottawa, Ottawa, Ontario K1N 6N5, Canada*
[3]*Regroupment Québécois sur les Matériaux de Pointe (RQMP), Département de physique, Université de Montréal, Québec, Canada H3C 3J7*
[4]*Institute for Microstructural Sciences, National Research Council, Ottawa, Ontario K1A 0R6, Canada*

(Received 25 October 2007; accepted 9 February 2008; published online 22 April 2008)

This work investigates the interdiffusion dynamics in self-assembled InAs/InP(001) quantum dots (QDs) subjected to rapid thermal annealing in the 600–775 °C temperature range. We compare two QD samples capped with InP grown at either optimal or reduced temperature to induce grown-in defects. Atomic interdiffusion is assessed by using photoluminescence measurements in conjunction with tight-binding calculations. By assuming Fickian diffusion, the interdiffusion lengths L_I are determined as a function of annealing conditions from the comparison of the measured optical transition energies with those calculated for InP/InAs$_{1-x}$P$_x$/InP quantum wells with graded interfaces. L_I values are then analyzed using a one-dimensional interdiffusion model that accounts for both the transport of nonequilibrium concentrations of P interstitials from the InP capping layer to the InAs active region and the P–As substitution in the QD vicinity. It is demonstrated that each process is characterized by a diffusion coefficient $D^{(i)}$ given by $D^{(i)}=D_0^{(i)}\exp(-E_a^{(i)}/k_BT_a)$. The activation energy and pre-exponential factor for P interstitial diffusion in the InP matrix are $E_a^{(\mathrm{P-InP})}=2.7\pm0.3$ eV and $D_0^{(\mathrm{P-InP})}=10^{3.6\pm0.9}$ cm^2 s^{-1}, which are independent of the InP growth conditions. For the P–As substitution process, $E_a^{(\mathrm{P-As})}=2.3\pm0.2$ eV and $(c_o/n_o)D_0^{(\mathrm{P-As})}\sim10^{-5}-10^{-4}$ cm^2 s^{-1}, which depend on the QD height and concentration of grown-in defects (c_o/n_o).
 [DOI: 10.1063/1.2905317]

I. INTRODUCTION

The expansion of optical communication networks motivates the development of materials suitable for laser sources and optical amplifiers in the infrared spectrum, which corresponds to the minimum absorption windows of glass fibers. Infrared materials and devices are also useful in a wide range of other fields, including atmospheric pollution control,[1] information processing and photodetection,[2] and biomedical applications.[3] Because of their emission around 1.5 μm and their zero dimensionality, InAs/InP quantum dots (QDs) are attractive materials for all of the above mentioned applications. However, the use of these nanostructures in practical devices relies on achieving precise control of their emission wavelength, which remains a challenge.

To overcome this issue, different band gap tuning techniques have been proposed: optimization of growth parameters,[4–7] introduction of interface layers,[8,9] and post-growth intermixing.[10–16] Intermixing is a thermally activated process that consists in atomic interdiffusion at the interface of materials with different alloy compositions. This process can be judiciously used to tune the emission properties of quantum heterostructures as it modifies their band gap and confinement profile, thus their corresponding energy levels.[10] The topic of locally enhanced interdiffusion has been receiving much attention since it can be used to finely tune the optoelectronic properties of heterostructures in specific regions of the sample for monolithic integration of planar waveguides[17] and optoelectronic components.[18] Enhanced intermixing during thermal treatment can be achieved through the localized creation or inclusion of point defects in the structure by using, for example, dielectric capping,[11] ion implantation,[12–15] or growth at reduced temperatures to introduce grown-in defects (GID).[16] Despite the success stories of these intermixing techniques, most of the work reported in literature have been essentially parametrical, demonstrating, for example, that a particular treatment can produce a certain amount of emission energy shift after annealing at a given temperature. Concerning GID-mediated intermixing, extended optical studies have been undertaken for In$_x$Ga$_{1-x}$As quantum wells (QWs) in GaAs by Khreis *et al.*[19] and in InP by Haysom *et al.*[20] They have demonstrated that the nonequilibrium concentration of GID—which is larger than the native defect concentration in thermal equilibrium—must be explicitly considered in analyzing and modeling intermixing experiments.

Despite its prime importance in better controling the optoelectronic properties of materials for technological applications, the interdiffusion dynamics in InAs/InP QDs remains poorly documented, even though these structures provide a remarkable system for fundamental studies. Indeed, since self-assembled QDs are statistically distributed in size, a

[a)]Also at the Institute for Microstructural Sciences, National Research Council, Ottawa, ON K1A 0R6 Canada. Electronic mail: carolyne.dion@polymtl.ca.

single sample can supply a variety of structure thicknesses grown under the same conditions, thereby allowing a systematic investigation of interdiffusion as a function of structure size by eliminating effects due to variations in templates or growth conditions. In this context, we have undertaken a study of the interdiffusion dynamics in InAs/InP QDs capped with an InP layer containing GID and subjected to rapid thermal annealing (RTA).

We have recently demonstrated by using a combination of photoluminescence (PL) experiments and tight-binding (TB) calculations that atomic intermixing occurring *during* the growth of InAs/InP QDs by chemical beam epitaxy (CBE) leads to the formation of alloyed QDs with relatively uniform composition.[21] For samples grown at ~500 °C, we have found that the composition of $InAs_{0.9}P_{0.1}$ provides the best description of measured transition energies. In the present article, we apply a similar procedure to investigate the interfacial intermixing caused by *post-deposition annealing*. Using the Fick diffusion formalism, we determine the diffusion length of intermixing, L_I, for annealed, intermixed QD structures. Inspired by the work of Khreis *et al.*[19] and Haysom *et al.*[20] on QWs, we analyze our data using a one-dimensional interdiffusion model taking into account the transport of P interstitials from the InP capping layer to the InAs active region and the P–As substitution at the QD vicinity. We demonstrate that intermixing in both sets of samples, i.e., those covered by an InP cap layer grown under optimal conditions as well as those in which the InP cap layer was grown at a reduced temperature to introduce GID, can be described by using this model, provided that nonequilibrium concentrations of P interstitials are considered. We determine the diffusion coefficients and activation energies associated with both P interstitial diffusion in InP and P–As substitution processes.

II. EXPERIMENTAL DETAILS

A. Experimental procedure

The samples were grown on semi-insulating Fe-doped InP(001) substrates by CBE from trimethylindium, arsine, and phosphine. The GID sample consisted of a 120-nm-thick InP buffer layer, 2.2 ML (monolayer) of InAs, which are followed by a 35 s growth interruption to allow QD formation, and a 40-nm-thick InP capping layer, which are all grown at 505 °C. The temperature was then ramped down to 450 °C for the growth of a 760-nm-thick InP layer. By doing so, a significant concentration of point defects was introduced into the epitaxial layer. Optimal conditions were then re-established for the growth of a 33-nm-thick InGaAs cap. The InGaAs layer was deposited in order to compensate for the low thermal stability of the low-temperature grown InP (LT-InP) and to avoid excessive surface degradation. For comparison with the GID sample, a standard (ST) sample was used. This sample consisted of a 125-nm-thick InP buffer layer, 2.9 ML InAs QD layer, which are followed by a 25 s growth interruption, and a 32-nm-thick InP capping layer, which are all grown at 515 °C. The temperature was then lowered to 500 °C for the growth of a 773-nm-thick InP layer. The samples were cleaved into approximately 5×5 mm^2 pieces, which were each subjected to anneals at constant annealing temperature (T_a) in the 600–775 °C range for incremental annealing times (t_a) of 60 s up to 300 s. RTA was carried out in a very large scale integrated grade N_2 atmosphere using an A.G. Associates Heatpulse 410 system with a thermocouple temperature control. During annealing, the GID and ST samples were respectively surrounded with sacrificial GaAs and InP pieces to minimize As or P desorption.

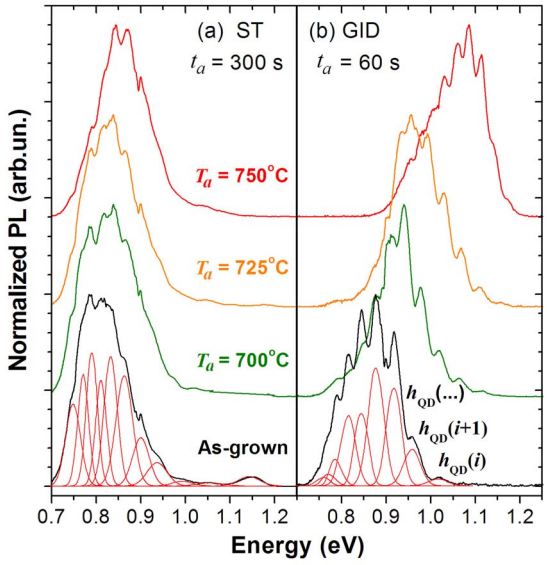

FIG. 1. (Color online) PL spectra at 77 K from the as-grown and annealed (a) ST and (b) GID samples as a function of annealing temperature T_a and time t_a.

PL measurements were performed at 77 K on as-grown samples and following each anneal using the 760 nm line of a Ti-sapphire laser as the excitation source. The incident light power density was kept constant at 200 W cm^{-2}, with the beam spot being 50 μm in diameter. This excitation power density proved to be sufficiently low to prevent any distortion of the spectra by excess carrier population in the QDs. The spectra were acquired using a double grating spectrometer and a cooled Ge detector. The resolution of the acquisition system was about 4 meV.

B. Photoluminescence results

Figures 1(a) and 1(b) show typical examples of normalized PL spectra from the as-grown and annealed ST and GID samples. The as-grown spectra are characterized by a wide emission band centered around 850 meV. Upon annealing, the overall QD emission spectra exhibit blueshifts, the magnitudes of which increase with T_a. Blueshifts of up to 120 and 210 meV can be obtained for the ST and GID samples, respectively. In all spectra, well-defined peaks are observed, which correspond to the fundamental electron–heavy-hole transitions (e1-hh1) of QD families with the same thicknesses in terms of an integer number of monolayers.[22]

The transition energies attributed to each QD family were extracted from every spectrum by using a multiparameter fit assuming a single Gaussian emission peak per QD family. As a starting point, the initial peak positions for the

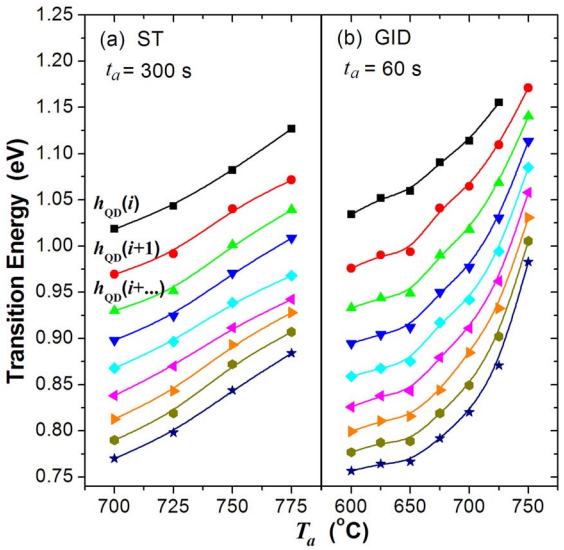

FIG. 2. (Color online) Evolution of the transition energy of the QD family peaks as a function of annealing temperature T_a for the (a) ST and (b) GID samples. The different symbols show the evolution of each QD family.

as-grown samples were estimated based on previous works,[21–24] while the full width at half maximum (FWHM) values were constrained to increase with increasing emission energy since interface roughness causes larger relative changes to the confinement emission energy in thinner QDs.[25] Examples of this fitting procedure are illustrated in Fig. 1 for the as-grown samples where the peaks are labeled in terms of QD height (h_{QD}) with incremental step of 1 ML. The peak energies obtained for the as-grown samples were then used to initialize the fit of the spectra from the annealed samples. A uniform shift was first applied to all transition energies and then individual peak positions and FWHMs were fitted to obtain the best match to each spectrum. Overall, this procedure allows the determination of the peak positions with less than 5 meV uncertainty. Figure 2 summarizes the results extracted from spectra such as those presented in Fig. 1.

The extracted optical transition energies were then compared to theoretical calculations for all of the samples, firstly to determine the initial state of the as-grown QDs and, secondly, to characterize the final P concentration profile of the intermixed QDs. In the following, we present more details of the PL analysis using the TB model.

III. PHOTOLUMINESCENCE ANALYSIS USING TIGHT-BINDING CALCULATIONS

Before investigating the influence of post-growth intermixing on the PL spectra, we must first analyze the emission characteristics from the as-grown samples. Through a combination of PL measurement and TB calculations, we have demonstrated in a previous work that significant intermixing takes place during the formation of InAs/InP QDs, leading to a blueshift of the emission spectra with respect to that expected from nominally pure InAs/InP QDs.[21] For the CBE samples investigated, the observed PL transitions were attributed to a 3-ML-thick wetting layer and 4 to 14-ML-thick QDs, with all the structures having essentially the same P concentration, ranging from 6% to 10% depending on the sample growth conditions. This conclusion was confirmed by Bloch-wave simulation of contrasts in plan-view transmission electron microscopy images. We have further argued that interdiffusion resulting from the high-temperature growth of the capping layers is negligible and that P incorporation in nominally pure InAs likely results from a combination of As/P exchange on the growth surface and strain-driven alloying, which lead to the formation of alloyed QDs with relatively uniform composition.

As in Ref. 21, we have used PL measurements and TB calculations to determine the h_{QD} values and P concentration of the as-grown ST and GID samples investigated in this study. In these calculations, the as-grown InAs/InP QDs are modeled by strained InP/$InAs_{1-x}P_x$/InP QWs with uniform P concentration and abrupt interfaces. As argued by various authors, the QW approximation is acceptable since the Coulomb and lateral confinement energies nearly cancel each other due to the small aspect ratio of these structures.[25,26] Details of the calculations as well as a discussion of the TB parametrization can be found in Ref. 27. The fundamental electron e1-hh1 transition energies are calculated by using the semi-empirical $sp^3d^5s^*$ nearest-neighbor TB model, the virtual crystal approximation, and the surface Green's function matching method. As is usual in TB calculations, the heterojunction band offset was taken into account by adding a constant value to the diagonal TB parameters. The unstrained valence band offset between InAs and InP was set to 0.35 eV, which is reasonable with respect to several results reported in the literature for the InAs/InP heterojunction.[27,28] The biaxial strain resulting from coherent growth on a substrate with a different lattice constant is evaluated by the macroscopic elasticity theory by using a linear approximation for the parameters of the $InAs_{1-x}P_x$ alloys. To allow a direct comparison between the experimental measurements realized at 77 K and those calculated at 0 K, a correction of the Bose–Einstein type of −3.5 meV was applied to the calculated values.[29] Similarly to the samples investigated in Ref. 21, we have found that the optical transitions from both the as-grown ST and GID samples presented in Fig. 1 arise from 5- to 13-ML-thick QDs with essentially the same P composition of [P]=9.5±0.7%.

By knowing the h_{QD} values and P concentration of the as-grown ST and GID samples, post-growth intermixing effects can now be determined. We suppose that these effects result in the formation of graded interfaces. Under Fick's diffusion formalism, by assuming a time-dependent (strain- and concentration-independent) interdiffusion coefficient D_I and an initial rectangular concentration profile using the as-grown QD conditions determined above, the solution of the P concentration profile (c_P) as a function of the position $\mathbf{z}$ (with respect to the center of the QD) and time t can be written as[30]

$$c_P(\mathbf{z},t) = \frac{[P]}{2}\left[\mathrm{erfc}\left(\frac{\mathbf{z}+h_{QD}/2}{L_I}\right)+\mathrm{erfc}\left(\frac{h_{QD}/2-\mathbf{z}}{L_I}\right)\right], \quad (1)$$

where L_I is the total interdiffusion length that depends on the interdiffusion coefficient D_I according to[19]

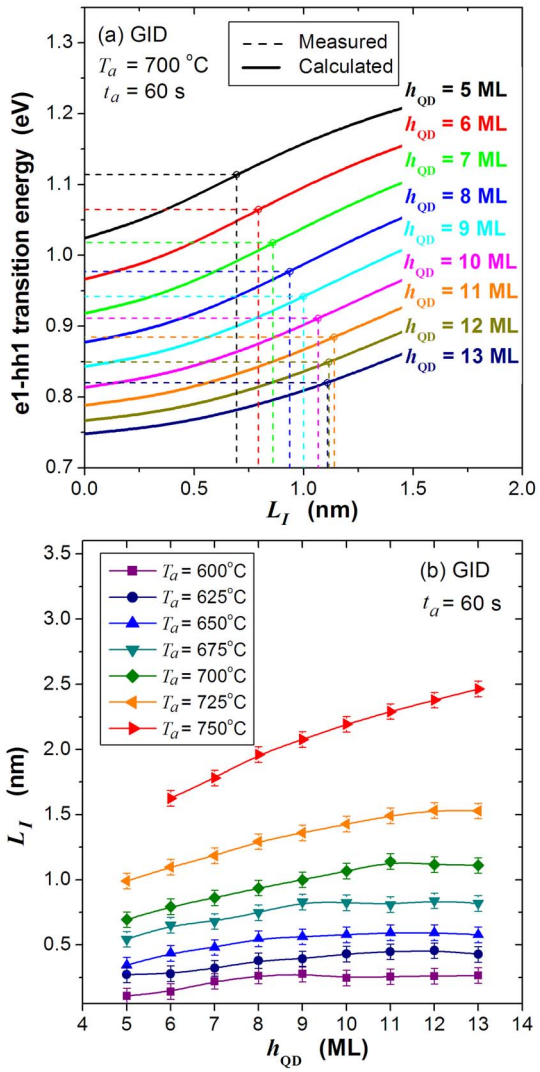

FIG. 3. (Color online) (a) Calculated e1-hh1 transition energies for various $InAs_{0.905}P_{0.095}$ QD thicknesses as a function of the interdiffusion length L_I. The values of L_I associated with each QD family are determined from the intersection between the calculated and measured optical transitions. Case shown: GID sample annealed at T_a=700 °C for t_a=60 s. (b) L_I determined for each QD family for a GID sample annealed at various annealing temperatures for t_a=60 s.

$$L_I^2 = 4\int_0^{t_a} D_I(t)dt. \tag{2}$$

The profile given by Eq. (1) was used as an input structure in the TB calculation model to determine transition energies as a function of L_I.

Figure 3 presents the e1-hh1 transition energies of interdiffused $InP/InAs_{0.905}P_{0.095}/InP$ QDs as a function of L_I and h_{QD}. For comparison with calculated results, the measured peak energies from each QD family were traced with horizontal solid lines and superimposed to the calculated transitions. From the intersections between the measured and calculated values, the interdiffusion length L_I was determined for each QD family and annealing conditions. This procedure is exemplified in Fig. 3(a) by using the optical transition energies for a GID sample annealed at T_a=700 °C for t_a=60 s. From the uncertainties in the optical transition energies, the error on L_I was estimated to be ±0.06 nm.

The interdiffusion lengths L_I were determined for each QD family and annealing conditions for both the ST and GID samples. As an example, Fig. 3(b) presents typical L_I results determined for each QD family within the GID sample annealed at various temperatures for t_a=60 s. This ensemble of data will be used in the next section to determine the interdiffusion coefficients, which provides insight into the interdiffusion dynamics.

IV. INTERDIFFUSION MODEL AND ANALYSIS

While a macroscopic treatment of diffusion through Fick's laws allows the determination of concentration profiles as a function of diffusion lengths, a microscopic approach is necessary to gain a fundamental understanding of the physical mechanisms driving the diffusion dynamics at the atomic scale. From an atomistic point of view, intermixing is governed by the transport of point defects, allowing the transition of atoms between adjacent sites. In the case of LT-InP, it has been established that these epitaxial layers have a P-rich stoichiometry with a large quantity of P_{In} antisite defects.[31,32] Upon annealing, these defects are expected to rapidly dissociate and release excess P interstitials.[33,34] These P interstitials diffuse from the LT-InP layer throughout the structure likely via interstitial or kick-out mechanisms.[20] Finally, P interstitials can cause composition change in the QDs via the kick-out mechanism with As atoms, producing at the same time As interstitials which undergo subsequent exchanges with the lattice P atoms. Frenkel interstitial-vacancy pairs can be also created in the structure upon high-temperature annealing, provided that atoms have enough energy to overcome the barrier required to escape from their site. This produces a uniform concentration of point defects in the structure. In contrast to the GID-mediated intermixing for which the transport of defects from the LT-InP layer to the active region plays an important role, the intermixing dynamics resulting from Frenkel pair defects is solely governed by the P–As substitution process because those defects are in thermal equilibrium.[30]

By assuming that interdiffusion dynamics is governed by P interstitial diffusion and P–As substitution, one can express the interdiffusion coefficient D_I as the product of P–As substitution coefficient $D^{(P-As)}$ and the fraction of interstitial sites occupied at the QD boundary layer.[19,30] This fraction is simply the concentration of interstitials, c_{int}, that is normalized to the total number of interstitial sites available, n_o.[30] The interdiffusion coefficient can thus be written as $D_I=(c_{int}/n_o)D^{(P-As)}$. It is common to suppose that c_{int}/n_o is constant for a given annealing temperature.[30,35–39] This implicitly assumes that Frenkel pairs are the dominant source of defects for intermixing. However, when the contribution of localized sources of defects such as GID becomes important, Khreis *et al.*[19] and Haysom *et al.*[20] showed that the time dependence of c_{int} resulting from the transport of defects must be considered. In order to determine which framework is the most appropriate for the samples investigated in the present work, we explore in the following both approaches—

equilibrium and nonequilibrium concentration of defects—in our analysis of the L_I values determined in Sec. III.

A. Equilibrium concentration of point defects

Let us first consider the case where defects responsible for intermixing are in thermal equilibrium. In such a case, the concentration of defects at the InAs/InP interface is independent of annealing time, so that Eq. (2) reduces to

$$L_I^2 = 4(c_{\text{int}}/n_o)D^{(\text{P–As})}t_a. \tag{3}$$

By assuming that P–As substitution is a thermally activated process, $D^{(\text{P–As})}$ depends on annealing temperature according to the Arrhenius relationship $D^{(\text{P–As})}=D_0^{(\text{P–As})}\exp(-E_a^{(\text{P–As})}/k_BT_a)$, where $E_a^{(\text{P–As})}$ and $D_0^{(\text{P–As})}$ are the activation energy and pre-exponential factor of the substitution process, and k_B is the Boltzmann constant. According to Eq. (3), plots of L_I^2 versus t_a should generate straight lines passing through the origin with slopes equal to $4(c_{\text{int}}/n_o)\ D^{(\text{P–As})}$.[35] Figures 4(a) and 4(b) present typical L_I^2 as a of function of t_a for the ST and GID samples. While both graphs do show within uncertainties the expected linear variation for each T_a, they also indicate T_a-dependent, non-zero intercepts.

Non-zero intercepts in intermixing investigations are normally attributed to the ramp and fall phases of the annealing cycles.[35–37] When a single sample is subjected to series of anneals of incremental, equal-time steps, the effect of the ramp and fall phases is identical for each anneal. This leads to a translation of L_I^2 versus t_a lines toward higher L_I^2 values, keeping the slope unchanged but giving a positive intercept.[36] By acknowledging this effect, we have performed least-squares analysis fits by using a general linear equation to extract the slopes providing the $(c_{\text{int}}/n_o)\ D^{(\text{P–As})}$ values.

Arrhenius plots of $(c_{\text{int}}/n_o)\ D^{(\text{P–As})}$ for different QD heights in the ST and GID samples are presented in Fig. 4(c). First, it can be seen that for a given sample, QD families present distinctive curves that are parallel to each other, with $(c_{\text{int}}/n_o)\ D^{(\text{P–As})}$ increasing with QD height. Secondly, it can be observed that the curves between the two sample sets are also parallel to each other. The latter two behaviors suggest that QD families in both the ST and GID samples are characterized by similar diffusion dynamics, hence similar activation energies.

Figure 4(c) further shows that the QD families for both types of the samples display convex Arrhenius relationships. As evidenced with bold lines, one can clearly distinguish a low-temperature regime for which $(c_{\text{int}}/n_o)\ D^{(\text{P–As})}$ exponentially decreases with increasing $1/T_a$. Least-squares fit in this regime reveal that both the ST and GID samples are characterized by $E_a^{(\text{P–As})}=2.9\pm0.5$ eV, with $D_0^{(\text{P–As})}$ being about 10^{-2} for ST and 10^{-1} cm^2 s^{-1} for GID. However, as the temperature increases, $(c_{\text{int}}/n_o)\ D^{(\text{P–As})}$ shows an increasing departure from the Arrhenius trend.

The deviations presented in Fig. 4(c) likely result from depletion in c_{int} at the QD vicinity. This could have been predicted in the case of the GID samples because the concentration of interstitials is likely to spatially and temporally vary.[19,20] However, the presence of deviations from the Arrhenius relation for the ST sample is in contradiction with the dominance of equilibrium defects generally assumed in such samples. In light of these results, we conclude that intermixing in both the ST and GID samples is governed by nonequilibrium concentrations of defects. Therefore, to precisely determine the parameters describing the intermixing process in such samples, in the next section, we develop a one-dimensional intermixing model allowing for the transport of interstitials from the InP cap layer to the InAs active region.

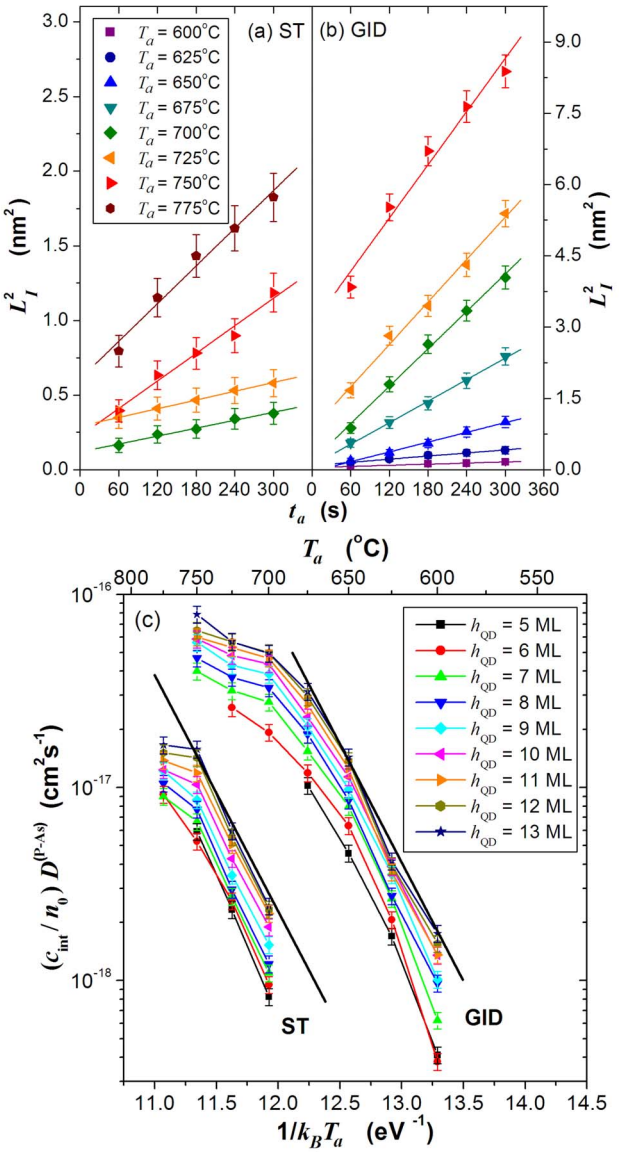

FIG. 4. (Color online) Square of the diffusion lengths extracted from the combined PL-TB procedure as a function of annealing time for different annealing temperatures for h_{QD}=8 ML in the (a) ST and (b) GID samples. The straight lines are the results of the linear fits. (c) Arrhenius plot of the interdiffusion coefficient for T_a between 600 and 775 °C for different QD families in GID and ST samples. The lines are guides to the eyes.

B. Nonequilibrium concentration of point defects

In the following, we consider the case where the concentration of interstitials at the QD boundary depends on the

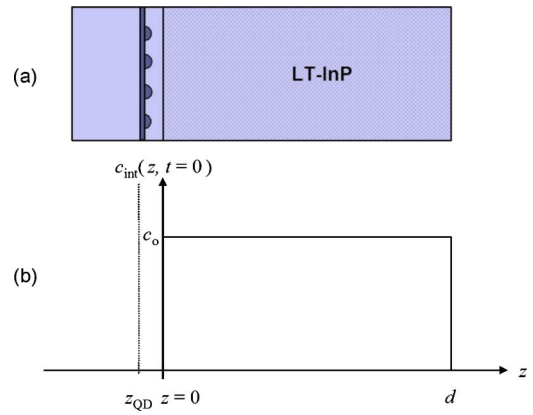

FIG. 5. (Color online) Schematic illustrations of (a) the geometry of the sample and (b) the initial defect concentration profile.

annealing time. We assume that P interstitials are essentially emanating from the InP capping layer grown at a reduced temperature. This is supported by the fact that the nonequilibrium concentration of GIDs in the LT-InP layer is significantly larger than the concentration of native defects in thermal equilibrium.[19] In this context, we consider that, initially, the interstitials are uniformly distributed throughout the LT-InP layer with thickness d such that

$$c_{\text{int}}(z,0) = \begin{cases} c_o, & 0 < z < d \\ 0, & z < 0. \end{cases} \tag{4}$$

Schematic illustrations of the sample geometry and initial defect concentration profile are shown in Fig. 5. For the ST sample, the QD position z_{QD} and LT-InP layer thickness d are, respectively, −32 and 773 nm. For the GID sample, $z_{\text{QD}}=-40$ nm and $d=760$ nm. By using the local-source solution of Fick's diffusion equations and the method of superposition (see the Appendix) with the initial conditions given in Eq. (4), the concentration of interstitial defects at position z and time t is

$$c_{\text{int}}(z,t) = \frac{c_o}{2}\left[\text{erf}\left(\frac{d-z}{\sqrt{4D^{(\text{P–In P})}t}}\right) - \text{erf}\left(\frac{-z}{\sqrt{4D^{(\text{P–In P})}t}}\right)\right], \tag{5}$$

where $D^{(\text{P–InP})}$ is the diffusion coefficient associated with the transport of P interstitials in the InP matrix.

By using Eq. (2) and knowing $c_{\text{int}}(z,t)$, the interdiffusion length can be written as

$$L_I^2 = 4D^{(\text{P–As})}(c_o/n_o)t_a\left\{a^2\left[\left(-1+\frac{\exp(-a^2)}{a\sqrt{\pi}}\right) + \left(1+\frac{1}{2a^2}\right)\text{erf}(a)\right] - b^2\left[\left(-1+\frac{\exp(-b^2)}{b\sqrt{\pi}}\right) + \left(1+\frac{1}{2b^2}\right)\text{erf}(b)\right]\right\}, \tag{6}$$

where $a=d-z_{\text{QD}}/L_{\text{P–InP}}$ and $b=-z_{\text{QD}}/L_{\text{P–InP}}$, with $L_{\text{P–InP}}=\sqrt{4D^{(\text{P–InP})}t_a}$ being the diffusion length associated with the transport of defects. Both P–As substitution and interstitial diffusion can be related to Arrhenius relationships, $D^{(i)}=D_0^{(i)}\exp(-E_a^{(i)}/k_BT_a)$, where $E_a^{(i)}$ and $D_0^{(i)}$ are the activation energy and pre-exponential factor of process i, where i=P–InP for interstitial diffusion or i=P–As for P–As substitution.

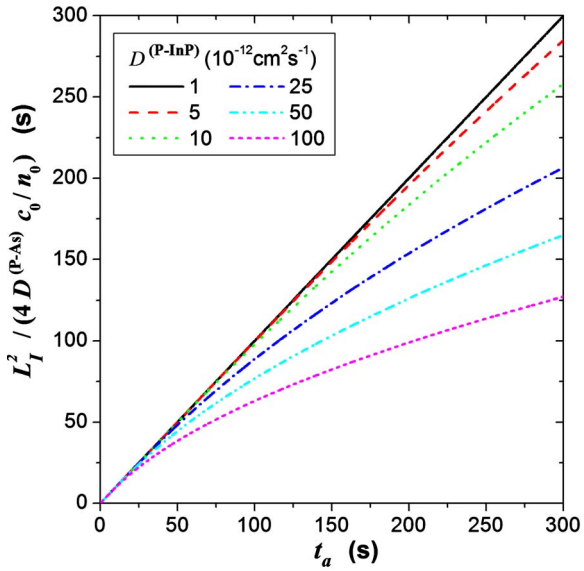

FIG. 6. (Color online) Normalized diffusion length squared as a function of time for $z_{\text{QD}}=0$ and $d=800$ nm.

When $|z_{\text{QD}}| \ll L_{\text{P–InP}} \ll d$, meaning that the QD layer is relatively close to the source of defects and that the InP capping layer is an interstitial reservoir far from depletion, Eq. (6) reduces to $L_I^2=2(c_o/n_o)D^{(\text{P–As})}t_a$. In that case, intermixing is solely governed by the P–As substitution process, similarly to Eq. (3), which is derived for defects in thermal equilibrium. On the other hand, when $L_{\text{P–InP}} \sim d$, meaning that interstitials easily diffuse out of the source that gradually becomes exhausted, intermixing depends on two thermally activated processes. Consequently, deviations from the linear dependence of L_I^2 with t_a arise. To better illustrate the implications of Eq. (6), Fig. 6 presents normalized diffusion lengths squared as a function of time for several values of $D^{(\text{P–InP})}$. Noticeable nonlinearities of L_I^2 with time can be observed as $D^{(\text{P–InP})}$ increases. For long annealing times ($t_a > 100$ s), all the curves appear roughly linear with their slope considerably decreasing with increasing $D^{(\text{P–InP})}$. This latter behavior clearly demonstrates that, as the transport of defects throughout the structure becomes important with respect to the dimensions of the system, the value of $D^{(\text{P–As})}$ determined via a simple linear fit of L_I^2 versus t_a is considerably underestimated. This is consistent with the appearance of a convex Arrhenius plot because $D^{(\text{P–InP})}$ is believed to increase with T_a.

Based on Eq. (6), we have reanalyzed the values of L_I^2 determined in Sec. III to extract (c_o/n_o) $D^{(\text{P–As})}$ and $D^{(\text{P–InP})}$ as a function of T_a and h_{QD}. We shall note that in order to get a satisfactory match to the experimental data, it was necessary to include the effects of the annealing ramp and fall phases in the form of non-zero intercepts. This was achieved by introducing in Eq. (6) an additional fitting parameter L_{I-0}^2 that was constrained to be the same for every h_{QD} in a given sample and to increase with increasing T_a. For instance, L_{I-0}^2 could take values between 0.05 and 1.5 nm^2. To illustrate the

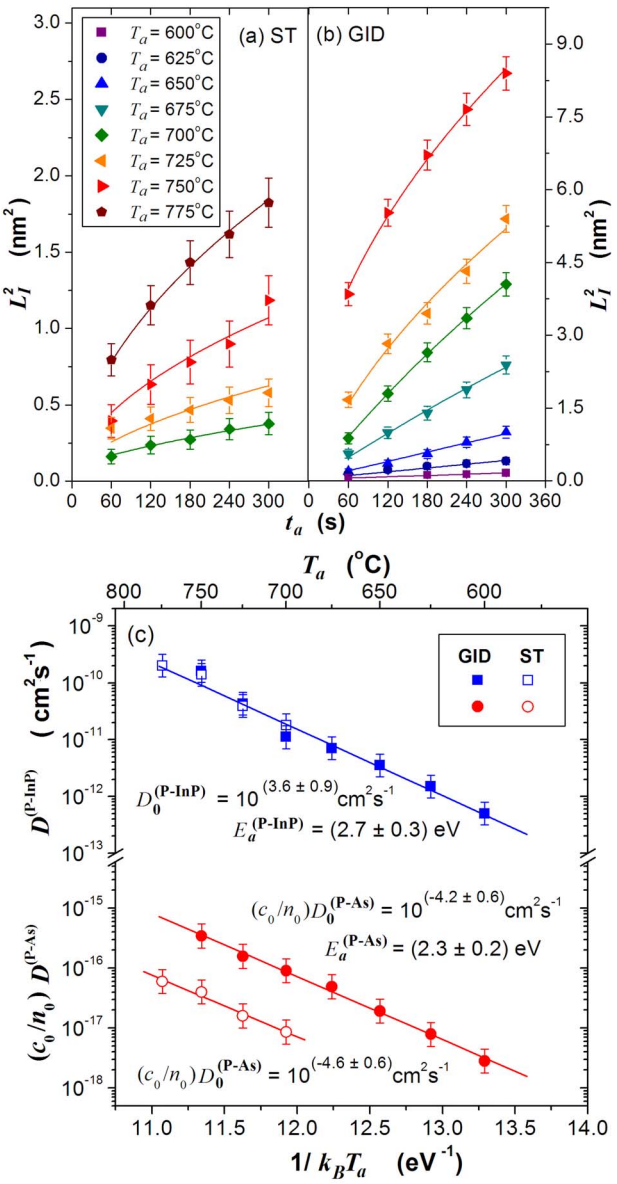

FIG. 7. (Color online) Square of diffusion lengths extracted from the combined PL-TB procedure as a function of annealing time for different annealing temperatures for h_{QD}=8 ML in the (a) ST and (b) GID samples. The lines are the results of the fitting procedure using Eq. (6). (c) Arrhenius plot of diffusion coefficients associated with the P–As substitution and defect transport for h_{QD}=8 ML in ST and GID samples. The straight lines are the results of the linear fits.

good agreement between the L_I^2 data and the model, an example of the fits is presented in Fig. 7 for h_{QD}=8 ML in the (a) ST and (b) GID samples.

The results of the fitting operation in Figs. 7(a) and 7(b) are presented in the Arrhenius plot of Fig. 7(c). In contrast with the results presented in Fig. 4(c), the diffusion coefficients related to the P–As substitution and the interstitial diffusion now follow an Arrhenius relationship for the entire temperature range investigated. By using a least-squares fit to each set of data, the P interstitial diffusion in InP and the P–As substitution processes are found to be characterized by activation energies of 2.3 ± 0.2 and 2.7 ± 0.3 eV, respectively. Figure 7(c) further shows that the ST and GID samples present $D_0^{(P\text{–}InP)} \sim 10^4$ cm^2 s^{-1}. The $(c_o/n_o)\ D_0^{(P\text{–}As)}$ values are found to be $\sim 10^{-5}$ cm^2 s^{-1} for the ST sample and $\sim 10^{-4}$ cm^2 s^{-1} for the GID. This difference can be probably explained by the variations in the initial concentration of defects, c_o. As a matter of fact, one expects the value of c_o to be higher in the GID samples than in the ST samples as a result of the lower growth temperature (450 versus 500 °C). Assuming that $D_0^{(P\text{–}As)}$ is similar for both the samples yields a factor 10 variation in c_o between the two samples. We shall note, however, that because of the lower melting point,[40] InP is less stable than InGaAs toward degradation during the RTA treatment. Therefore, variation in the concentration of defects, c_o, may be related not only to the InP growth temperature but also to the composition of the topmost capping layer. As a final remark, we also note that the activation energies and pre-exponential factors presented above appear reasonable because they are of the same order as those reported by other authors for In(Ga)As/In(Ga)AsP/InP QWs, which vary between 2.5 and 3.8 eV and between 10^{-5} and 23 cm^2 s^{-1}, respectively.[39,41]

The pre-exponential factors and activation energies associated with defect transport and P–As substitution processes determined from the Arrhenius plot are presented in Figs. 8(a) and 8(b) as a function of the QD height for the GID sample. The values of $E_a^{(P\text{–}InP)}$, $E_a^{(P\text{–}As)}$, and $D_0^{(P\text{–}InP)}$ are fairly constant (within the error bars) but do show a tendency to increase with h_{QD}. In contrast, $(c_o/n_o)\ D_0^{(P\text{–}As)}$ clearly increases from $\sim 10^{-5}$ to 10^{-3} cm^2 s^{-1} with h_{QD}.

We shall discuss the possible phenomena at the origin of this behavior. First, based on Eq. (6), by considering that $E_a^{(P\text{–}As)}$ is the same for all QD families and that c_o is constant for a given sample, $D_0^{(P\text{–}As)}$ must increase with h_{QD}. This increase in the pre-exponential factors can be possibly attributed to compressive strain accumulation around the QDs, producing a local enhancement of the concentration of mobile interstitials.[42] Indeed, it has been demonstrated that interstitial diffusivity increases with hydrostatic pressure.[43] Accordingly, the strain in the InP capping layer due to the presence of QD creates an accelerating field for interstitial diffusion. Because the extent of the strain field in InP is roughly proportional to the QD height,[44,45] defects traveling from the top to the bottom would be subjected to the accelerating strain field of the taller QDs before that of thinner dots. A larger number of defects would therefore reach the surroundings of taller structures, which enhances the rate of intermixing. On the other hand, P-concentration-dependent $D^{(P\text{–}As)}$ could produce a decrease in the pre-exponential factor with decreasing h_{QD}. However, we expect the latter effect to be negligible since we were successful in describing the time and annealing temperature dependence of L_I in the InAs/InP system without taking this phenomenon into account. Finally, the evolution of the prefactor and the activation energy could be also related to the Meyer–Neldel (MN) or compensation law.[46] This phenomenon has been observed in a wide range of thermally activated processes, particularly in those involving activation energies which are large compared with the energies of excitations, normally infrared vibrations, or phonons, and with the temperature of the system. In these conditions, a large number of excitations must occur for the process to take place so that multiexcitation entropy

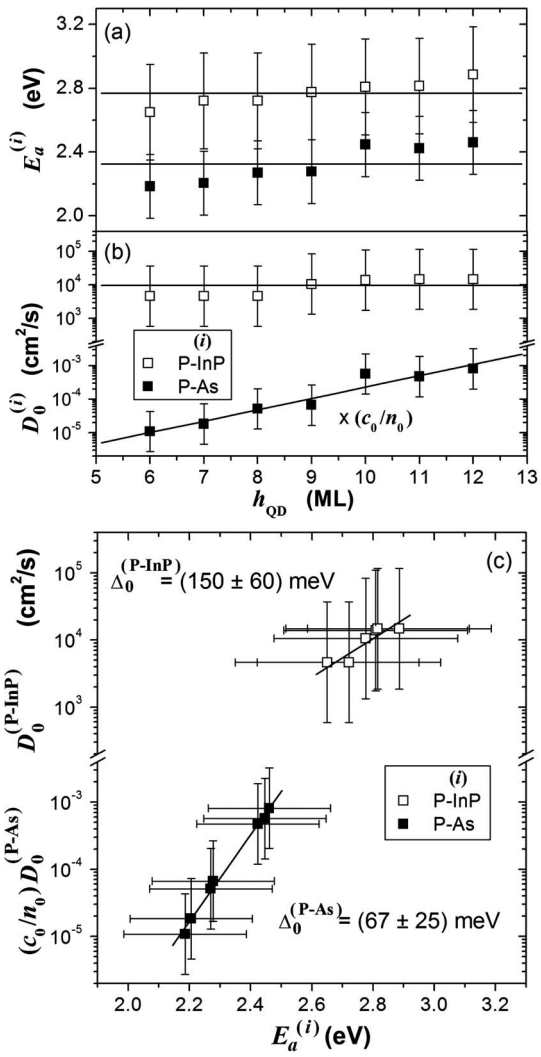

FIG. 8. (a) Activation energies and (b) pre-exponential factors associated with the interstitial transport in InP and P–As substitution processes as determined for the various QD families in the GID sample. (c) The MN plot of the pre-exponential factor vs the activation energy from the data presented in (a) and (b).

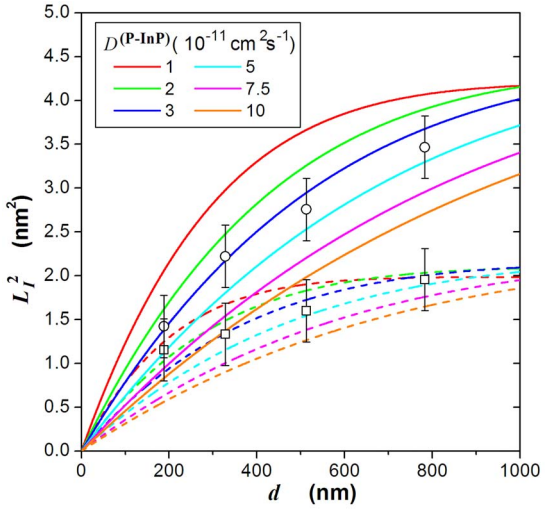

FIG. 9. (Color online) Square of the diffusion length obtained from the PL transition energies from InAs/InP QDs following anneals at T_a=725 °C for t_a=60 s (open squares) and t_a=120 s (open circles) reported in Ref. 16. The results from Eq. (6), using $D^{(P\text{–}As)}=10^{-16}$ cm^2 s^{-1}, are also presented for comparison.

effects must be taken into account. Using the usual formulation of the MN law, $D_0=D_{00}\exp(E_a/\Delta_0)$ in which Δ_0 is the MN energy, in Fig. 8(c), we plot the values of $D_0^{(P\text{–}As)}$ and $D_0^{(P\text{–}InP)}$ as a function of $E_a^{(P\text{–}As)}$. Despite the large uncertainties, the MN seems to be obeyed for both $D_0^{(P\text{–}As)}$ and $D_0^{(P\text{–}InP)}$, with Δ_0 being in the usually reported 25–200 meV range.[46]

In the previous sections, intermixing was studied as a function of annealing time and temperature for a constant source of defects. In order to further validate the importance of defect transport in the interdiffusion dynamics, we have carried out an extended analysis on another series of samples for which the LT-InP capping layer thicknesses are varied. More precisely, we have re-examined the PL transition energies from InAs/InP QDs following anneals at T_a=725 °C for t_a=60 and 120 s reported in Ref. 16 as a function of the thickness of the LT-InP capping layer. PL measurements were analyzed by using the approach described in Sec. III to extract the experimental values of L_I. Theoretical L_I^2 were evaluated from Eq. (6) for different $D^{(P\text{–}InP)}$ values by using the $(c_o/n_o)\,D^{(P\text{–}As)}$ value of 2×10^{-16} cm^2 s^{-1}, as shown in Fig. 7(c), for the GID sample at T_a=725 °C. Figure 9 presents the theoretical and experimental L_I^2 values determined as a function of d. First, Fig. 9 shows that for given $L^{P\text{–}InP}$, i.e., a given t_a and $D^{(P\text{–}InP)}$, the L_I^2 values monotonically increase with d and reach a plateau when $d \gg L_{P\text{–}InP}$. One can see the excellent agreement between the experimental and theoretical results for $D^{(P\text{–}InP)}\sim3\times10^{-11}$ cm^2 s^{-1}, which corroborates with the obtained diffusion coefficient in Fig. 7(c). In addition, this value corresponds to the defect diffusion coefficient determined by Haysom *et al.*[20] from their intermixing study in InGaAs/InP QWs, which is $\sim10^{-11}$ cm^2 s^{-1}. This provides additional evidence for the importance of considering the transport of the nonequilibrium concentration of defects from a localized source.

V. CONCLUSION

In conclusion, we have investigated the interdiffusion process of InAs/InP QDs capped with an InP layer containing GID and subjected to RTA. PL analysis and TB calculations were jointly used to extract the interdiffusion lengths of intermixed structures over a wide range of annealing times and temperatures. When considering a constant concentration of defects in the QD vicinity for the analysis of the interdiffusion lengths, the P–As substitution process was found to be characterized by the apparent convex Arrhenius relationship $(c_{int}/n_o)\,D^{(P\text{–}As)}$, suggesting that c_{int} is not constant as is commonly assumed. The time dependence of the defect concentration in the intermixing model can be accounted for by considering that the InP capping layer acts as a source of highly mobile P interstitials, which promote intermixing in the QD region. Under this model, standard linear Arrhenius relationships were obtained for both P interstitial diffusion and P–As substitution. The activation energy and pre-exponential factor for P interstitial diffusion in

InP were found to be $E_a^{(\mathrm{P-InP})}=2.7\pm0.3$ eV, and $D_0^{(\mathrm{P-InP})}=10^{3.6\pm0.9}$ cm^2 s^{-1}. For the P–As substitution process, $E_a^{(\mathrm{P-As})}=2.3\pm0.2$ eV, while the $(c_o/n_o)\,D_0^{(\mathrm{P-As})}$ values ranged from 10^{-5} to 10^{-4} cm^2 s^{-1}, which depends on the QD height and defect concentration. Moreover, the ST and GID samples were found to be described by similar $D^{(\mathrm{P-InP})}$ and $E_a^{(\mathrm{P-As})}$ values. From the results of this work, we conclude that in both the ST and GID InAs/InP QD samples, intermixing is governed by the concentration of nonequilibrium P interstitials in the InP capping layer. The primary difference between the different samples essentially resides in the concentration of defects, c_o, which is a strong function of the growth conditions.

ACKNOWLEDGMENTS

The authors acknowledge the National Science and Engineering Research Council of Canada, the National Research Council of Canada, and the Canada Research Chair program for financial support. The authors also acknowledge Professor Arthur Yelon for insightful discussions.

APPENDIX: DETERMINATION OF THE CONCENTRATION PROFILE

We assume that the defects promoting interdiffusion originate only from the InP capping layer grown at a reduced temperature. Thus, the initial distribution of defects can be represented by a uniform distribution of line sources following

$$c_{\mathrm{int}}(z,0)=\begin{cases} c_o, & 0<z<d \\ 0, & z<0, \end{cases} \tag{A1}$$

where d is the thickness of the capping layer. A schematic is presented in Fig. 10.

To determine the defect concentration profile during anneal, we use the local-source solution of the diffusion equation to build up the solution for the finite initial distribution by superposition. The amount of diffusing material contributed by each source can be written as $c_o d\xi$. Now, let us consider the contribution at an arbitrary position z from a source at some other position ξ. The distance between these locations is $\xi-z$; thus, the diffusion concentration profile related to this source can be written as

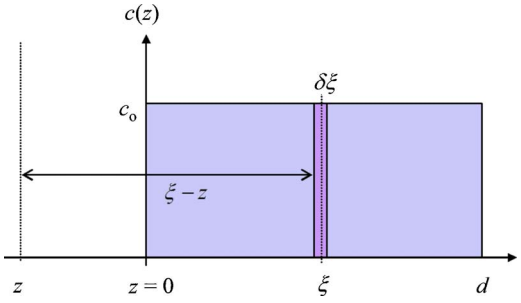

FIG. 10. (Color online) Initial defect concentration profile used in the determination of the solution of the one-dimensional diffusion problem.

$$c_{\text{int-}\xi}(z,t)=\frac{c_o d\xi}{\sqrt{4\pi D^{(\mathrm{P-InP})}t}}\exp\left[-\left(\frac{\xi-z}{\sqrt{4D^{(\mathrm{P-InP})}t}}\right)^2\right], \tag{A2}$$

where $D^{(\mathrm{P-InP})}$ is the diffusion coefficient associated with the transport of defects. The general solution corresponding to the conditions given by Eq. (A1) is the integral over all planar sources, such as

$$c_{\mathrm{int}}(z,t)=\frac{c_o}{\sqrt{4\pi D^{(\mathrm{P-InP})}t}}\int_0^d \exp\left[-\left(\frac{\xi-z}{\sqrt{4D^{(\mathrm{P-InP})}t}}\right)^2\right]d\xi. \tag{A3}$$

By transferring the integration variable by using $u=(\xi-z)/\sqrt{4D^{(\mathrm{P-InP})}t}$, we find

$$c_{\mathrm{int}}(z,t)=\frac{c_o\sqrt{4D^{(\mathrm{P-InP})}t}}{\sqrt{4\pi D^{(\mathrm{P-InP})}t}}\int_{-z/\sqrt{4D^{(\mathrm{P-InP})}t}}^{d-z/\sqrt{4D^{(\mathrm{P-InP})}t}} \exp(-u^2)du. \tag{A4}$$

By using the relationship, $\int_\alpha^\beta \mathrm{epx}(-u^2)du=\sqrt{\pi}/2[\mathrm{erf}(\beta)-\mathrm{erf}(\alpha)]$, Eq. (A4) becomes

$$c_{\mathrm{int}}(z,t)=\frac{c_o}{2}\left[\mathrm{erf}\left(\frac{d-z}{\sqrt{4D^{(\mathrm{P-InP})}t}}\right)-\mathrm{erf}\left(\frac{-z}{\sqrt{4D^{(\mathrm{P-InP})}t}}\right)\right], \tag{A5}$$

which is the resulting concentration profile for the finite initial distribution assumed above. The time integrated concentration can be analytically solved, which gives

$$\int_0^{t_a} c_{\mathrm{int}}(z,t)dt=c_o t_a\left\{a^2\left[\left(-1+\frac{\exp(-a^2)}{a\sqrt{\pi}}\right)+\left(1+\frac{1}{2a^2}\right)\mathrm{erf}(a)\right]-b^2\left[\left(-1+\frac{\exp(-b^2)}{b\sqrt{\pi}}\right)+\left(1+\frac{1}{2b^2}\right)\mathrm{erf}(b)\right]\right\}, \tag{A6}$$

where $a=d-z/\sqrt{4D^{(\mathrm{P-InP})}t_a}$ and $b=-z/\sqrt{4D^{(\mathrm{P-InP})}t_a}$.

[1] Y. Zaatar, J. Bechara, A. Khoury, D. Zaouk, and J.-P. Charles, Appl. Energy **65**, 107 (2000).
[2] E. Towe and D. Pan, IEEE J. Sel. Top. Quantum Electron. **6**, 408 (2000).
[3] P. H. Tomlins and R. K. Wang, J. Phys. D **38**, 2519 (2005).
[4] P. J. Poole, R. L. Williams, J. Lefebvre, and S. Moisa, J. Cryst. Growth **257**, 89 (2003).
[5] B. J. Riel, K. Hinzer, S. Moisa, J. Fraser, P. Finnie, P. Piercy, S. Fafard, and Z. R. Wasilewski, J. Cryst. Growth **236**, 145 (2002).
[6] B. Wang, S.-J. Chua, Z. Wang, and S. Liu, Physica E (Amsterdam) **8**, 290 (2000).
[7] P. Paki, R. Leonelli, L. Isnard, and R. A. Masut, J. Appl. Phys. **86**, 6789 (1999).
[8] S. Barik, H. H. Tan, and C. Jagadish, Nanotechnology **17**, 1867 (2006).
[9] S. Barik, H. H. Tan, C. Jagadish, N. Vukmirovic, and P. Harrison, Appl. Phys. Lett. **88**, 193112 (2006).
[10] J. F. Girard, C. Dion, P. Desjardins, C. N. Allen, P. J. Poole, and S. Raymond, Appl. Phys. Lett. **84**, 3382 (2004).
[11] C. K. Chia, S. J. Chua, S. Tripathy, and J. R. Dong, Appl. Phys. Lett. **86**, 051905 (2005).
[12] D. Nie, T. Mei, C. D. Xu, and J. R. Dong, Appl. Phys. Lett. **89**, 131103 (2006).
[13] S. Barik, H. H. Tan, and C. Jagadish, Appl. Phys. Lett. **88**, 223101 (2006).
[14] C. Dion, P. Desjardins, M. Chicoine, F. Schiettekatte, P. J. Poole, and S.

Raymond, Nanotechnology **18**, 15404 (2007).
[15]S. Barik, H. H. Tan, and C. Jagadish, Appl. Phys. Lett. **90**, 093106 (2007).
[16]C. Dion, P. J. Poole, S. Raymond, P. Desjardins, and F. Schiettekatte, Appl. Phys. Lett. **89**, 131905 (2006).
[17]J. H. Marsh, J. Cryst. Growth **288**, 2 (2006).
[18]J. Nah and P. Likamwa, Opt. Quantum Electron. **38**, 567 (2006).
[19]O. M. Khreis, W. P. Gillin, and K. P. Homewood, Phys. Rev. B **55**, 15813 (1997).
[20]J. E. Haysom, P. J. Poole, R. L. Williams, S. Raymond, and G. C. Aers, Solid State Commun. **116**, 187 (2000).
[21]C. Dion, P. Desjardins, N. Shtinkov, M. D. Robertson, F. Schiettekatte, P. J. Poole, and S. Raymond, Phys. Rev. B **77**, 075338 (2008).
[22]S. Raymond, S. Studenikin, S.-J. Cheng, M. Pioro-Ladriere, M. Ciorga, P. J. Poole, and M. D. Robertson, Semicond. Sci. Technol. **18**, 385 (2003).
[23]J. M. Sallese, S. Taylor, H. J. Buhlmann, J. F. Carlin, A. Rudra, R. Houdre, and M. Ilegems, Appl. Phys. Lett. **65**, 341 (1994).
[24]Y. Sakuma, M. Takeguchi, K. Takemoto, S. Hirose, T. Usuki, and N. Yokoyama, J. Vac. Sci. Technol. B **23**, 1741 (2005).
[25]H. Folliot, S. Loualiche, B. Lambert, V. Drouot, and A. LeCorre, Phys. Rev. B **58**, 10700 (1998).
[26]C. Cornet, C. Levallois, P. Caroff, H. Folliot, C. Labbe, J. Even, A. Le Corre, S. Loualiche, M. Hayne, and V. V. Moshchalkov, Appl. Phys. Lett. **87**, 233111 (2005).
[27]N. Shtinkov, P. Desjardins, and R. A. Masut, Phys. Rev. B **66**, 195303 (2002).
[28]I. Vurgaftman, J. R. Meyer, and L. R. Ram-Mohan, J. Appl. Phys. **89**, 5815 (2001).
[29]L. Malikova, F. H. Pollak, R. A. Masut, P. Desjardins, and L. G. Mourokh, J. Appl. Phys. **94**, 4995 (2003).
[30]R. W. Balluffi, S. M. Allen, and W. C. Carter, *Kinetics of Materials* (Wiley-Interscience, New York, 2005).
[31]D. P. Docter, J. P. Ibbetson, and Y. Gao, Conference Proceedings of the International Conference on Indium Phosphide and Related Materials, p. 53 (1998).
[32]P. Dreszer, W. M. Chen, K. Seendripu, J. A. Wolk, W. Walukiewicz, B. W. Liang, C. W. Tu, and E. R. Weber, Phys. Rev. B **47**, 4111 (1993).
[33]K. Karsten and P. Ehrhart, Phys. Rev. B **51**, 10508 (1995).
[34]H. Hausmann and P. Ehrhart, Phys. Rev. B **51**, 17542 (1995).
[35]W. P. Gillin, D. J. Dunstan, K. P. Homewood, L. K. Howard, and B. J. Sealy, J. Appl. Phys. **73**, 3782 (1993).
[36]W. P. Gillin, J. Appl. Phys. **85**, 790 (1999).
[37]O. M. Khreis, Solid State Commun. **132**, 767 (2004).
[38]Y. Kajikawa, N. Nishimoto, D. Fujioka, and K. Ichida, Jpn. J. Appl. Phys., Part 1 **45**, 2412 (2006).
[39]H. Peyre, F. Alsina, J. Camassel, J. Pascual, and R. W. Glew, J. Appl. Phys. **73**, 3760 (1993).
[40]M. Levinshtein, S. Rumyantsev, and M. Shur, *Handbook Series on Semiconductor Parameters* (World Scientific, London, 1996), Vol. 1 and 2.
[41]W. P. Gillin, S. S. Rao, I. V. Bradley, K. P. Homewood, A. D. Smith, and A. T. R. Briggs, Appl. Phys. Lett. **63**, 797 (1993).
[42]H. S. Djie, D.-N. Wang, B. S. Ooi, J. C. M. Hwang, X.-M. Fang, Y. Wu, J. M. Fastenau, and W. K. Liu, J. Appl. Phys. **100**, 03527 (2006).
[43]M. J. Aziz, Y. C. Zhao, H. J. Gossmann, S. Mitha, S. P. Smith, and D. Schiferl, Phys. Rev. B **73**, 054101 (2006).
[44]H. J. Chu and J. Wang, J. Appl. Phys. **98**, 034315 (2005).
[45]V.-G. Stoleru, D. Pal, and E. Towe, Physica E (Amsterdam) **15**, 131 (2002).
[46]A. Yelon, B. Movaghar, and R. S. Crandall, Rep. Prog. Phys. **69**, 1145 (2006).